INFLOW AND THE FATIGUE OF THE LIST WIND TURBINE*†

Herbert J. Sutherland
Wind Energy Technology Department
Sandia National Laboratory
Albuquerque, NM 87185-0708
hjsuthe@sandia.gov

ABSTRACT

The Long-term Inflow and Structural Test (LIST) program is collecting long-term, continuous inflow and structural response data to characterize the spectrum of loads on wind turbines. A heavily instrumented Micon 65/13M turbine with SERI 8m blades is being used as the primary test turbine for this test. This turbine is located in Bushland, TX, a test site that exposes the turbine to a wind regime representative of a Great Plains commercial site. The turbine and inflow are being characterized with 60 measurements: 34 to characterize the inflow, 19 to characterize structural response, and 7 to characterize the time-varying state of the turbine. In this paper, the inflow and structural data from this measurement campaign are analyzed to determine the correlation of various inflow descriptors with fatigue loads. The inflow is described by various parameters, including the mean, standard deviation, skewness and kurtosis of the wind speed, turbulence intensity, turbulence length scales, Reynolds stresses, local friction velocity, Obukhov length and the gradient Richardson number. The fatigue load spectrum corresponding to these parameters is characterized as an equivalent fatigue load. A regression analysis is then used to determine which parameters are correlated to the fatigue loads. The results illustrate that the vertical component of the inflow is the most important of the secondary inflow parameters on fatigue loads. Long-term fatigue spectra illustrate that extrapolation of relatively short-term data to longer times is consistent for the data reported here.

INTRODUCTION

The Long-term Inflow and Structural Test (LIST) program [1,2] is collecting long-term, continuous inflow and structural response data. The program is designed to characterize the extreme loads on the turbine and to determine the influence of various atmospheric parameters on fatigue loads.

To characterize the spectrum of these low-occurrence events requires a long-term, time-synchronized database that characterizes both the structural responses of the wind turbine and the inflow for at least a wind season. Previous studies have examined the influence of various inflow parameters on structural response. However, most of these studies are typically too short to find the extremes, or they have limited inflow data. One notable exception is the study reported by Glinou and Fragoulis [3]. In this detailed study, multiple turbines in complex mountain terrain are characterized with large arrays of inflow and structural measurements. Their work is serving as a guide for the LIST program.

This paper presents a detailed analysis of the influence of secondary inflow parameters on fatigue loads imposed upon the LIST turbine. The analysis is based on inflow and structural measurements that span a total of 333 hours (1998 ten-minute records) with average hub-height wind speeds up to almost 19 m/s. The data set was first divided into wind speed bins. All records below the cut-in wind speed were discarded, leaving a total of 1017 10-minute data records between 5 and 19 m/s. These records were then divided into Wind Speed Classes based on their mean wind speed. This manuscript concentrates on the approximately 20 hours (118 records) of Wind Speed Class 5 (11 to 13 m/s) data.

A total of 18 inflow parameters are examined here: two primary inflow parameters [mean hub-height wind speed and turbulence (turbulence intensity)] and 16 "secondary" inflow parameters that have been proposed by various researchers. All 18 parameters were determined for each 10-minute record and the fatigue loads measured in each record were characterized as an equivalent fatigue load over a range of fatigue exponents. The records were then sorted and binsed by mean wind speed. Using a multi-variable regression analysis on the equivalent fatigue loads, the influence

*Sandia is a multiprogram laboratory operated by Sandia Corporation, a Lockheed Martin company, for the U.S. Department of Energy under contract DE-AC04-94AL85000.

of each secondary inflow parameter on fatigue loads was determined for each wind speed bin. The primary inflow parameters were excluded from the regression analysis. The results of this analysis illustrate that the vertical component of the inflow is the most important of the secondary inflow parameters on fatigue loads.

Long-term fatigue spectra were also examined. These data illustrate that extrapolation of relatively short-term data to longer times is consistent for the data reported here.

THE LIST TURBINE

The turbine used in this experimental investigation is a Micon 65/13M turbine. A complete description of the turbine, its site, and instruments used to monitor the turbine and its inflow are provided by Sutherland, Jones and Neal [1]. A synopsis of this description is provided here for completeness.

The Turbine

The turbine used in this experimental investigation is a modified Micon 65/13 turbine (65/13M), see Fig. 1. This turbine is a fixed-pitch, 3-bladed up-wind turbine with a three-phase 480 V asynchronous generator rated at 115 kW. The generator operates at 1200 rpm while the blades turn at a fixed 55 rpm (the standard Micon 65/13 turbine rotates at a fixed 45 rpm).

The turbine is fitted with Phoenix 8m blades that are based on Solar Energy Research Institute (SERI)[‡] airfoils. These "SERI" blades are 7.9 m (312 in) long and are equipped with tip brakes.

This turbine is located with two similar turbines on the USDA Agriculture Research Service (ARS) site in Bushland, TX. This site is characteristic of a Great Plains site with essentially flat terrain. The primary wind direction at the site is from 215° with-respect-to True North. The wind rosette for this site shows a secondary peak for winds from approximately due North.

Instrumentation

The turbine and its inflow are monitored using 60 sensors: 34 to characterize the inflow, 19 to characterize structural response, and 7 to characterize the time-varying state of the turbine.

Fig. 1. The Micon 65/13M Turbine at the Bushland Test Site.

Primary inflow measurements are obtained using 5 3-axis sonic anemometers located 1.8 diameters upwind (with-respect-to the prevailing winds) of the turbine. Four of these anemometers are placed about a circle, whose diameter is equal to that of the rotor, at the top, bottom, left and right extremities. The final anemometer, located at the center of the circle, is aligned with the rotor hub. These detailed inflow measurements are augmented using cup anemometers and wind vanes placed strategically about the site.

The turbine's structural response is monitored primarily using strain gauges that are clustered on the blade and the hub. Additional measurements include tower moments and nacelle accelerations.

Turbine state measurements include rotor position and speed, yaw position, power production and grid connection (on-off switch).

[‡] SERI is now the National Renewable Energy Laboratory (NREL).

Data System

The instruments cited above are monitored continuously using the Accurate, Time-Linked Data Acquisition System, ATLAS, described in detail by Berg and Zayas [4]. The system monitors a total of 75 channels: 60 instrument channels and 15 time and status channels. The clocks on the system maintain a 1 micro-second accuracy using satellite links to the GPS system.

The data stream is monitored at a rate of 30 Hz. This yields a Nyquist Frequency of 15 Hz, which is sufficient for capturing the behavior of the inflow and the structural response of the turbine. ATLAS uses a second-order anti-aliasing active filter followed by a programmable fifth-order Butterworth filter. The cut-off frequency for the latter filter was set to 15 Hz.

The data system automatically segments the data into 10-minute blocks, converts the data into engineering units, and archives them for future processing.

THE DATA SET

The distribution of the 1017 ten-minute records contained in the current data set is summarized in Fig. 2. As illustrated by this figure, the records have been divided into wind speed classes for this analysis. Wind speed bin class 3 encompasses speeds to 9 m/s (the sum of the first two columns in Fig. 2). Bin classes 4, 5, 6 and 7 encompass speed ranges of 9-11, 11-13, 13-15 and 15-17 m/s, respectively. Bin class 8 encompasses all wind speeds above 17 m/s. As illustrated in this figure, 186 records are above 11 m/s mean wind speed. No 10-minute record has a mean wind speed above 19 m/s.

FORMULATIONS

The Inflow Parameters

Over the past few years, many inflow parameters have been proposed as having influence over the fatigue loads on a wind turbine. The mean wind speed and turbulence (or turbulence intensity) are the most widely recognized as having the major influence on loads. Additional proposed parameters have been summarized to a large extent by Rohatgi and Nelson [5], Fragoulis [6] and Glinou and Fragoulis [3]. Additional parameters have been proposed by Kelley [7, 8]. Sixteen (16) of these secondary parameters are examined here.

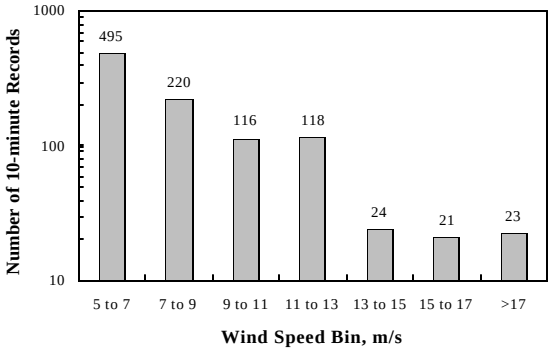

Fig. 2. Distribution of the 10-minute Data Records by Hub-Height Mean Wind Speed.

Justifying the inclusion or exclusion of a parameter in this list and detailing its physical significance is beyond the scope of this paper. Rather, the purpose of this paper is to continue to quantify their influence on turbine fatigue loads. As the quantifying process continues, many of these parameters will be discarded and others added.

The symbols and underlying mathematical formulations for the various inflow and structural parameters are presented in the Appendices.

Equivalent Fatigue Load

The equivalent fatigue load [9, 10] is used to quantize the fatigue damage contained in spectral load distributions contained in each 10-minute record. In general, the equivalent fatigue load is determined using Miner's Rule to combine the spectral components into a single, constant-rate fatigue load that will produce equivalent damage. For the case of a constant mean (range-only cycle counts) and a power law S-N curve with a fatigue exponent of m [10, 11], the equivalent cyclic load F_e has the form:

$$F_e = \left[\frac{\sum_i (F_i)^m \, n_i}{N_o} \right]^{1/m} , \qquad [1]$$

where F_e is the load to failure at a total of N_o fatigue cycles.

The choice of N_o is somewhat arbitrary. It is sometimes chosen to be a number of cycles suitable for laboratory testing, i.e., 10^6 cycles [9]. Other times, it is

chosen to be approximately the average number of cycles recorded in the data set; i.e., the average number of cycles in a 10-minute data set. If data are not available, then the choice of N_o is typically based upon the rotational frequency f_o of the turbine [3,10]. Since the choice of N_o is essentially arbitrary and does not influence the comparative nature of the analysis presented here, we will assume a constant value for N_o of 2000 cycles for the equivalent-fatigue-load data analysis.

As illustrated in Eq. 1, F_e is not unique for a given load spectra. Not only does it depend on the choice of N_o, but it also depends on the fatigue exponent m. For comparison purposes, F_e is usually reported for multiple values of m. Typical values for m are 3 for welded steel, 6 for extruded aluminum and 10 for fiberglass composite materials.

For the analysis presented here, the initial fatigue spectrum (range-only cycle counts) was determined by rainflow counting the bending moment data in each mean wind speed bin using CRUNCH [12]. The resulting cycle counts were then reduced to an equivalent fatigue load using Eq. 1, the assumed value for N_o and three values of m.

Multi-Variable Fitting Routine

The multi-variable fitting routine used to fit the various inflow parameters to the equivalent fatigue load is based on the general linear least squares routine described by Press, Teukolsky, Vetterling and Flannery [13]. Their routine determines a generalized fit to a set of points (x_i,y_i) for the basis functions X_k by determining values for the parameters a_k which minimize the merit function χ^2:

For a basis function of the form:

$$\hat{y}(x) = \sum_{i=1}^{M} a_k \; X_k(x) \quad , \qquad [2]$$

then the merit function becomes

$$\chi^2 = \sum_{i=1}^{N} \left[\frac{y_i - \sum_{k=1}^{M} a_k \; X_k(x_i)}{\sigma_i} \right] \quad , \qquad [3]$$

where σ_i is the measurement error (standard deviation) of the i^{th} data point. If the measurement errors are not known, they may all be set to the constant value of one [13].

The basis functions are arbitrary fixed functions of x; they are not necessarily polynomials. As pointed out by the authors of this algorithm: "…, if you are willing to tolerate a bit of programming hack," the generalized fitting techniques they employ may be expanded from the dependence on a single variable x to a dependence on a vector variable **x**, i.e., a set of variables x_k.

For the analysis presented here, the basis function for each variable that composes the vector $\mathbf{x} = (x_1, x_2, \ldots, x_M)$ was assumed to be a polynomial of the form:

$$X_k(x_k) = \sum_{j=1}^{P} a_{kj} \; x_k^j \quad , \qquad [4]$$

and the measurement error σ_i was assumed to be one, see Eq. [3]. For these assumptions, Eq. 3 becomes:

$$\chi^2 = \sum_{i=1}^{N} \left\{ y_i - \hat{y}(x) \right\} \quad , \qquad [5]$$

where

$$\hat{y}\left[X_k(x_k) \right] = a_o + \sum_{k=1}^{M} \sum_{j=1}^{P} a_{kj} \; x_k^j \quad . \qquad [6]$$

In the Mounturb report [3], the value of P was taken to be 1, i.e., a linear fit. With this additional assumption, Eq. 6 becomes:

$$\hat{y}(x) = a_o + a_1 \; x_1 + a_2 \; x_2 + \ldots + a_M \; x_M \quad . \qquad [7]$$

The form shown in Eq. [7] is the one used in the analysis presented here.

Dependence Coefficient

To quantify the influence of each inflow parameter on fatigue loads requires the development of a "dependence coefficient." The one proposed by Glinou and Fragoulis [3] is "the relative per sigma dependence coefficient S_k for each parameter. For a linear formulation, see Eq. 7, S_k has the following form:

$$S_k = a_k \frac{\sigma_{x_k}}{\bar{y}} \quad . \qquad [8]$$

Thus, S_k measures the normalized effect of increasing the k^{th} parameter by one standard deviation, with the result normalized by the mean value of the dependent variable y

DEPENDENCE OF INFLOW PARAMETERS

As known throughout the wind industry, the primary inflow parameters that influence turbine fatigue damage are the mean wind speed and turbulence (turbulence intensity). Outlined above and in the Appendices are a large number of secondary inflow parameters that may also influence fatigue loads. Of these proposed parameters, a total of 16 secondary parameters are examined here; the influence of the two primary parameters is not examined here. Using the analyses described above, the dependence of the equivalent fatigue load for flap and edge bending loads on each of these parameters was determined for three fatigue exponents. Typical results for the dependence of the equivalent fatigue load on the 16 inflow parameters are shown in Fig. 3.

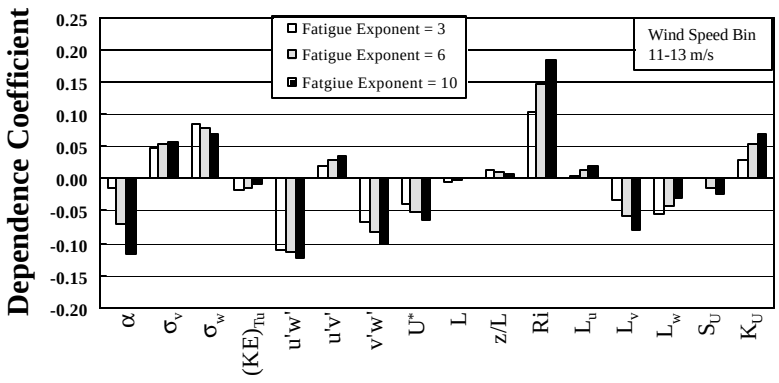

Fig. 3a. Flap Bending Loads.

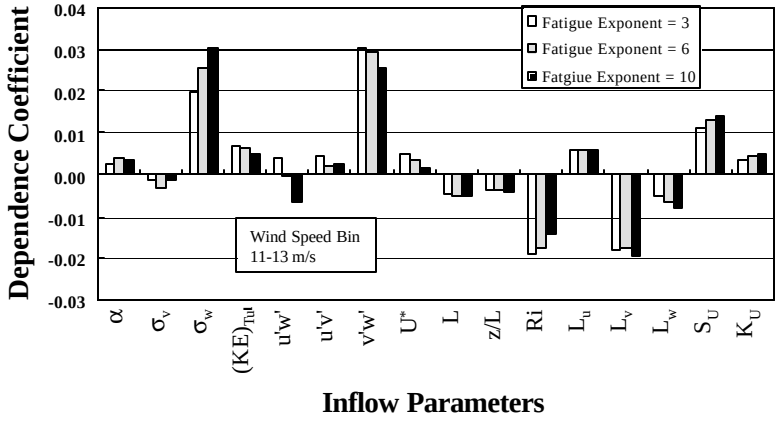

Fig. 3b. Edge Bending Loads.

Fig. 3. Dependence of Equivalent Fatigue Load on Various Inflow Parameters for Class 5 (11-13 m/s) Wind Speeds.

Class 5 Wind Speeds

The results shown in Fig. 3 are for Class 5 wind speeds (11 to 13 m/s), see Fig. 2. The analysis is based on 118 10-minute records. In this analysis, the linear, multi-variable fit was used.

As shown in Fig. 3a, the Richardson number is the most important of the group of inflow variables examined here for flap bending. It is followed closely by the cross-velocity Reynolds stresses, $u'w'$ and $v'w'$, and the vertical shear exponent α. For edge bending, see Fig. 3b, the $v'w'$ Reynolds stress and the standard deviation of the vertical wind component σ_w (i.e., a measure of the vertical turbulence), are the most important, followed by the Richardson number and the cross-rotor, horizontal turbulence length scale, L_v. Note that the correlation of the edge fatigue loads to all of the inflow parameters is significantly less than that of the flap loads.

Additional Wind Speed Classes

Plots of the dependence coefficient for flap bending in other wind speed classes are shown in Figs. 4, 5, 6 and 7. These analyses are based upon 116, 24, 21 and 23 10-minute records, respectively.

As shown in these figures, the dependency of the equivalent fatigue load varies widely across the wind

speed classes. The general trend is less dependency of the Richardson number and more dependency on the various terms that depend on the cross velocities v and, especially, w. In particular, the local friction velocity, u*, becomes predominant.

Similar results have been found for edge bending.

Summary

The vertical component of the inflow arises as the most-important characteristic of the inflow that influences fatigue loads. A description of this parameter in terms of the secondary inflow parameters is cross-velocity Reynolds stresses and the local friction velocity. Similar results are reported by Fragoulis [6]. The atmospheric stability term, Richardson number, also plays an important role.

LONG-TERM FATIGUE LOAD SPECTRUM

One of the long-term objectives of the LIST program is to obtain long-term fatigue spectra for the turbine blade loads. The long-term fatigue spectra for 118 10-minute records in wind class 5 offer an important database for studying long-term fatigue spectrum. These data are summarized in Figs. 8 and 9.

In these two figures, the fatigue spectra are typical spectra for this class of turbines. Namely, the edge-bending spectra display a bi-modal distribution, see Figs. 8a and 9a, that is directly attributed to the large 1P gravity component of the bending moment, see Sutherland [2]. As illustrated in Figs. 8b and 9b, the fatigue spectrum for flap-bending moment has a very different character, with a single-mode distribution.

In Fig. 8, the 20-hour data is contrasted to the 1-hour data reported by Sutherland [2]. In Fig. 9, the data are contrasted to the 1-hour and the 7-hour data. These comparisons illustrate the importance of long-term data sets. In particular, the 1-hour data spectra have a so-called "floor" occuring at approximately 1 cycle count per hour. This floor is easily observed in the data presented in Fig. 8a and b in bins above approximately 25 kNm and 30 kNm, respectively. As the bins that constituent the floor of the data contains only a single cycle count, using them as an estimate of the long-term behavior would not be accurate because the

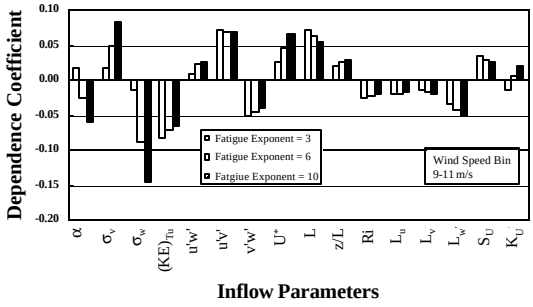

Fig. 4. Dependence of Equivalent Fatigue Load on Various Inflow Parameters for Class 4 Wind Speeds.

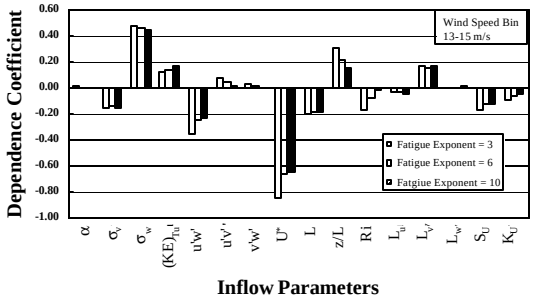

Fig. 5. Dependence of Equivalent Fatigue Load on Various Inflow Parameters for Class 6 Wind Speeds.

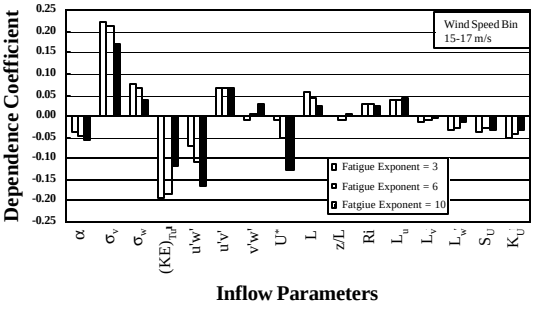

Fig. 6. Dependence of Equivalent Fatigue Load on Various Inflow Parameters for Class 7 Wind Speeds.

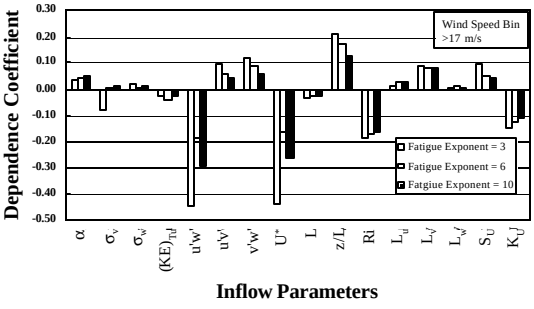

Fig. 7. Dependence of Equivalent Fatigue Load on Various Inflow Parameters for Class 8 Wind Speeds.

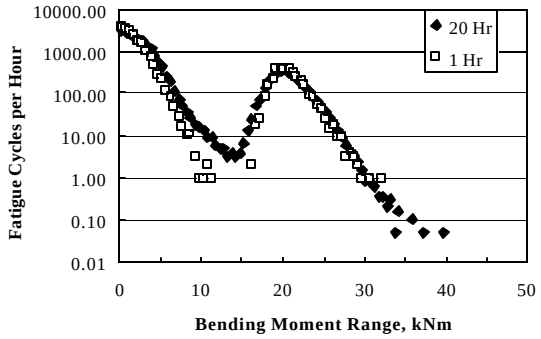

Fig. 8a. Edge-Bending in the Root of Blade 1.

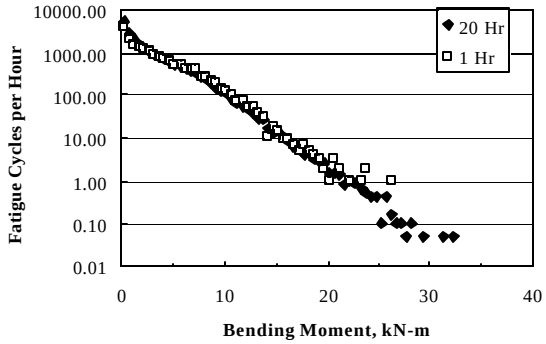

Fig. 8b. Flap-Bending in the Root of Blade 1.

Fig. 8. Fatigue Load Spectrum for Class 5 Wind Speeds.

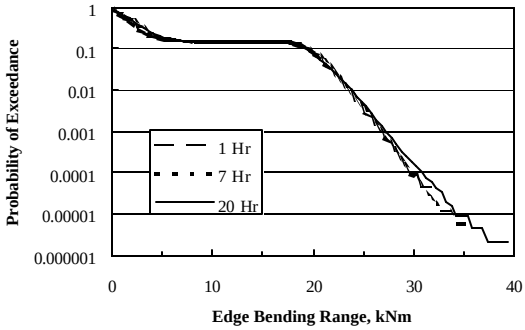

Fig. 9a. Edge-Bending in the Root of Blade 1.

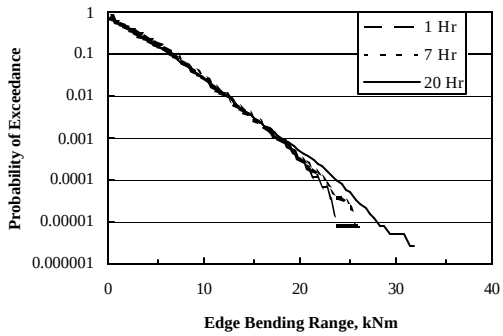

Fig. 9b. Flap-Bending in the Root of Blade 2.

Fig. 9. Exceedance Plots of the Fatigue Load Spectrum for Class 5 Wind Speeds.

number of observations is not statistically significant.

When more data are added, in this case approximately 19 hours of data are added, the floor is lowered to approximately 0.0525 cycles per hour, i.e., one cycle in approximately 20 hours. In both the edge and the flap bending cases, the 7-hour exceedance curve lies virtually on top of the 1-hour curve until the floor in the 1-hour data set is reached.

The significant difference between the various data sets is that the expansion of the data set to 20 hours extends the exceedance curve to a new floor. In particular, the additional data indicates that the primary slope of the exceedance curve in the high bending moment region of the spectrum continues unabated past the floor of the 1-hour data set.

These data indicate that the extrapolation of relatively short-term spectra to long-term spectra is consistent with measured data. And, based on the data analyzed here, the high-stress tail of the distribution continues to at least a floor of 1 count in 20 hours, with no end in sight.

LOAD EXTREMES

The extreme loads are one of the major drivers in the design of wind turbines. The time-synchronized data provided by LIST provides a detailed look at these events.

Long-Term Ultimate Loads

Madsen, Pierce and Buhl [14] have addressed the statistical uncertainty of loads prediction using structural dynamics simulation codes. The data presented in Fig. 10 offer measured-data that may be used to examine load extremes for the operating wind turbine.

The extreme loads are shown in Fig. 10 for Class 5 wind speeds. For edge bending loads, the mean value is 18.55 kNm with a standard deviation of 1.52 kNm; i.e., a COV (ratio of the standard deviation to the mean) of

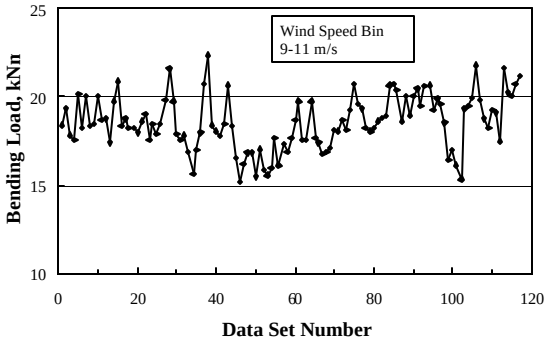

Fig. 10a. Edge-Bending Loads.

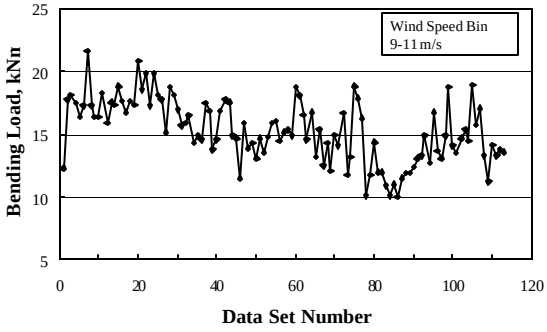

Fig. 10b. Flap-Bending Loads.

Fig. 10. Load Extremes for Class 5 Wind Speeds.

8.21 percent. For flap, these values are 15.28 kNm, 2.47 kNm, and 16.17 percent, respectively. Following the lead of Madsen et. al. [14], these measured values can be statistically extrapolated to design conditions.

Flow Field

As the inflow and the structural loads are time synchronized, a detailed examination of the inflow conditions that produced these extremes can be made from the measured data. To illustrate this dimension in the LIST data, consider the extreme flap-bending load observed in the seventh data set, see Fig. 10b. This data set was taken on May 14, 2000, starting at approximately 40 seconds past noon. The average, hub-height wind speed in this 10-minute record was 12.38 m/s with a turbulence intensity of 15.23 percent. The extreme occurred at approximately 23.7 seconds into the record.

The flap bending record for this event is shown in Fig. 11. Various measurements of the inflow at the time of the event are also shown in this figure. The time of the event has been delineated with a vertical dashed line in all of these records. For the inflow measurements, the position of the event has not been shifted forward in time to account for the transport time of approximately 2 seconds.[§]

As seen in this figure, the horizontal wind speed component at the centerline of the turbine is well above the average wind speed for the 10-minute record. At the time of the event, the vertical wind speed component at the hub is reversing direction. The horizontal wind speed component is approximately 5 m/s less at the bottom of rotor than at the top, and approximately 4 m/s less of the right side of the rotor than on the left side. Thus, the rotor is seeing a strong shear field in both the horizontal and vertical directions, plus the vertical wind speed is oscillating between positive (up) and negative (down). Although this situation does not appear to be unique, even in the 20 seconds of data presented here, the result is a strong spike in the flap loads.

Timing

The data presented in Fig. 11 indicate that the conditions producing the extreme were prevalent for approximately 6 seconds before the extreme was actually reached. These conditions produced a succession of strong spikes in the load histogram (at approximately 19 21, 22 and 23 seconds into the record), that culminated in the final, largest load spike. Thus, extrema would appear to be clustered in time.

From a fatigue standpoint, the clustering of extrema is not as important as the elapsed time between the largest loads and the smallest loads (over all data records). These are the peaks and valleys that are combined by the rainflow counting algorithm to form the large ranges found in the tail of the fatigue-cycle distribution, see Figs. 8 and 9. Using the extreme load plot for the Class 5 wind speeds shown in Fig. 10 and a similar plot of the extreme minimum values, the timing of the extreme fatigue cycles can be ascertained. In particular, the extreme maximum edge-bending load occurred approximately 43 hours before the extreme minimum edge-bending load. For flap-bending loads, the extreme maximum occurred approximately 94.5 hours before the extreme minimum. The extremes for edge and flap

[§] The inflow instrumentation is located approximately 30.7 m in front of the turbine. Thus, with an average hub-height velocity of over 15 m/s, inflow events occur approximately 2 seconds before a measured structural event.

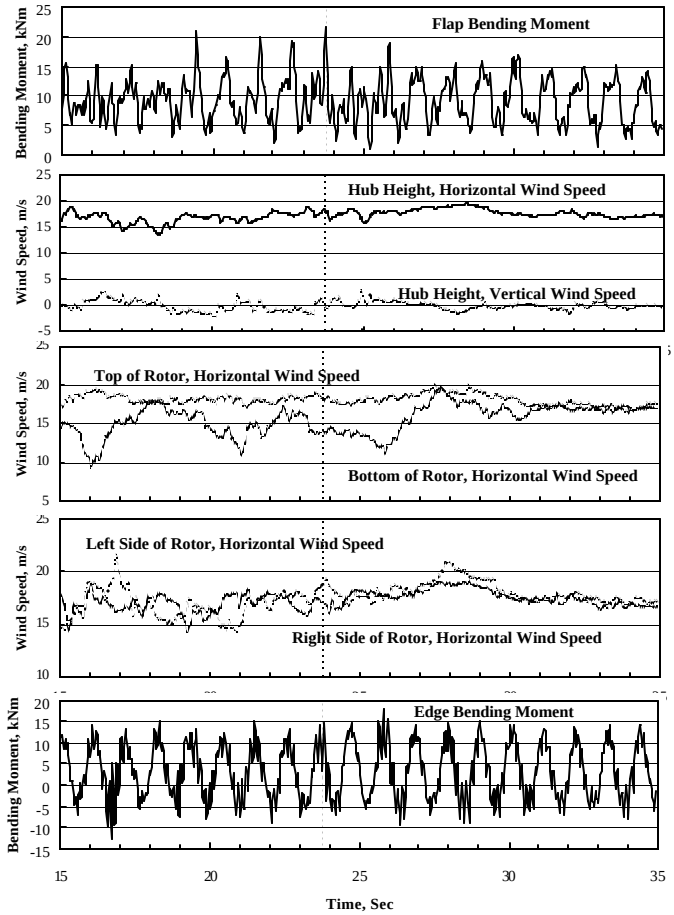

Fig. 11. Flow Field and Structural Measurements about the Extreme Flap Event for Class 5 Wind Speeds.

bending did not occur at the same time or even in the same 10-minute record.

Thus for this data set, the elapsed time between extreme peaks and valleys is not sufficient to warrant concern about the effect of material memory on the high-stress cycles in the tail of the fatigue cycle distribution.

CONCLUDING REMARKS

The long-term data set from the LIST program has been used to examine the influence of various secondary inflow parameters on the fatigue loads on a turbine. Based upon a multi-variable regression analysis of the equivalent fatigue load, terms involving the vertical component of inflow velocity and the Richardson Number consistently have the most influence. Long-term fatigue spectra illustrate that extrapolations of relatively short-term data are consistent with long-term measured data.

For the analysis presented here, only proposed inflow parameters have been explored. However, the wealth of data contained in the LIST data set offers many more possible combinations: debatably, the most important being the spatial correlations across the rotor of the horizontal and vertical components of the inflow.

ACKNOWLEDGEMENTS

The data used in the analysis is the direct results of a dedicated team of researchers. The author wishes to thank the LIST Team for their efforts. The author also wishes to thank Neal Kelley, NREL, for supplying many of the discretized formulations for the various inflow variables presented in Appendix A.

REFERENCES

[1]. Sutherland, H.J., P.L. Jones, and B. Neal, 2001, "The Long-Term Inflow and Structural Test Program," *2001 ASME Wind Energy Symposium*, AIAA/ASME, pp. 162-172.

[2]. Sutherland, H.J., 2001, "Preliminary Analysis of the Structural And Inflow Data From the LIST Turbine," *2001 ASME Wind Energy Symposium*, AIAA/ASME, pp. 173-183.

[3]. *Mounturb Final Report*, 1996, G. Glinou and A. Fragoulis, eds., 3 vols., JOU2-CT93-0378.

[4]. Berg, D., and J. Zayas, 2001, "Accurate Time-Linked Data Acquisition System Field Deployment and Operational Experience," *2001 ASME Wind Energy Symposium*, AIAA/ASME, pp. 153-161.

[5]. Rohatgi, J.S., and V. Nelson, 1994, *Wind Characteristics, An Analysis for the Generation of Wind Power*, Alternative Energy Institute, Canyon, TX, 237 p.

[6]. Fragoulis, A.N., 1997, "The Complex Terrain Wind Environment and Its Effects on the Power Output and Loading of Wind Turbines," *1997 ASME Wind Energy Symposium*, AIAA/ASME, pp. 33-40.

[7]. Kelley, N.D., and H.E. McKenna, 1996, "The Evaluation of a Turbulent Loads Characterization System." *1996 ASME Wind Energy Symposium*, ASME, pp. 69-77.

[8]. Kelley, N.D., A.D. Wright, M.L. Buhl, Jr., and J.L. Tangler, 1997, "Long-Term Simulation of Turbulence-Induced Loads Using the SNL WINd-3D, FAST, YawDyn, and ADAMS Numerical Codes," *1997 ASME Wind Energy Symposium*, ASME, pp. 74-85.

[9]. *Wind Turbine Generator Systems, Part 13: Measurement of Mechanical Loads*, Draft Technical Report, 1998, IEC 61400-13, prepared by IEC-TC88, Working Group 11.

[10]. Sutherland, H.J., 1999, *On the Fatigue Analysis of Wind Turbines*, SAND99-0089, Sandia National Laboratories, Albuquerque, NM, 132 p.

[11]. Musial, W., M. Clark, N. Egging and M. Zuteck, 1997, "A Comparison of Strength and Load-Based Methods for Testing Wind Turbine Blades," *1997 ASME Wind Energy Symposium*, AIAA/ASME, W. Musial and D.E. Berg, eds., p. 228.

[12]. Buhl, M.L., Jr., 2001, *CRUNCH User's Guide*, Ver. 2.61, NREL/NWTC, Golden, CO, 11 p.

[13]. Press, W.H., S.A Teukolsky, W. T. Vetterling and B.P. Flannery, 1992, *Numerical Recipes in C, The Art of Scientific Computing*, Second Edition, Chapter 15.4, Cambridge University Press.

[14]. Madsen, P.H., K. Pierce and M. Buhl, 1999, "Predicting Ultimate Loads for Wind Turbine Design," *1999 ASME Wind Energy Symposium*, AIAA/ASME, T. Ashwill, ed., p. 355.

APPENDIX A

NOMENCLATURE

Symbols

a — Regression coefficients, see Eq. [3]

F_e — Equivalent fatigue load, see Eq. [1]

f_o — Rotational frequency of the turbine

g — Acceleration of gravity, 9.8 m/s^2

I — Turbulence intensity (percent)

$$\sigma_U / U \qquad [A\text{-}1]$$

$(KE)_{Tu}$ — Turbulence kinetic energy,

$$\tfrac{1}{2}\left[(u')^2 + (v')^2 + (w')^2\right] \quad , \qquad [A\text{-}2]$$

L — Obukhov length:

$$\frac{-\overline{\theta_s}\, u_*^3}{0.4\, g\, \overline{(w'\theta_s')}} \quad , \qquad [A\text{-}3]$$

L_u, L_v, L_w — Turbulence length scales in the u, v, and w directions (m)

$$L_u = \overline{U_s} \int_0^T R_{u'}(\tau)\, d\tau \quad , \qquad [A\text{-}4]$$

M, N, P — Counting indexes

m — Material constant, exponent for the S-N curve

N_o — Cycle to failure at load F_e, see Eq. [1]

P — Barometric pressure, (hPa) at height z_1

P_s — Height corrected pressure

$$P_s = P_1 - \left[\frac{0.0341416\, P_1}{\Theta_1 + 273.16}\right](z_s - z_1) \qquad [A\text{-}5]$$

R — Autocorrelation function

Ri — Gradient Richardson number:

$$\frac{g}{\theta_m}\,\frac{\Delta\theta}{(\Delta U)^2} \quad , \qquad [A\text{-}6]$$

S — Dependence Coefficient, see Eq. 8

t — Time

T — Total period of time

u, U — Horizontal wind speeds (m/s)

u* — Local friction velocity, (m/s)

$$-\left|\sqrt{\overline{u'w'}}\right| \qquad [A\text{-}7]$$

$\overline{u'w'}$, $\overline{u'v'}$, $\overline{v'w'}$ — Reynolds stresses, (m^2/s^2)

v Instantaneous horizontal wind vector component, perpendicular to the average horizontal wind direction Φ_H (m/s)

w Instantaneous vertical wind vector component, perpendicular to the average total wind direction Φ_T (m/s)

x, **x** Independent variable in regression analysis, see Eq. [3]

X Basis functions in regression analysis, see Eq. [3]

y Dependent variable in regression analysis, see Eq. [3], measured value

$\hat{y}$ Dependent variable in regression analysis, see Eq. [3], calculate value from curve fit

z Vertical height (m)

α Vertical wind shear exponent:

$$U_z / U_{Hub} = \left[z / z_{Hub} \right]^{\alpha} \quad , \qquad [A\text{-}8]$$

Δ Gradient over distance, see Eq. B-4

ϕ Wind direction (degrees with-respect-to True North)

Θ Temperature, °C

θ Pressure-corrected absolute temperature, °K

$$\theta_s = \left(\Theta_s + 273.16\right) \left[\frac{1000}{P_s} \right]^{0.286} \qquad [A\text{-}9]$$

τ Integration parameter on time

$\mathcal{X}$ Merit function in regression analysis, see Eq. [3]

Subscripts

1, 2 Vertical positions 1 and 2

H Horizontal

i, j, k Counting indexes

m Average over distance, see Eq. B-3

T Total

Tu Turbulence

U Horizontal Wind Speed at Hub Height

s Sonic

Superscripts

' Instantaneous value with the mean removed, see below

APPENDIX B

GENERAL EQUATIONS

$\overline{X}$ Mean value of X over time period t:

$$\overline{X} = \frac{1}{T} \int_0^T x(\tau)\, d\tau = \frac{1}{N} \sum_{i=1}^{N} x_i \quad , \qquad [B\text{-}1]$$

X' Fluctuation component of X:

$$x'(t) = x(t) - \overline{X} \quad , \qquad [B\text{-}2]$$

X_m Mean over two elevations:

$$X_m = \frac{\left(X_1 + X_2\right)}{2} \quad , \qquad [B\text{-}3]$$

ΔX Differential in the vertical direction:

$$\Delta X = \frac{X_2 - X_1}{z_2 - z_1} \quad , \qquad [B\text{-}4]$$

σ_x Standard deviation;

$$\sqrt{\frac{1}{N} \sum_{i=1}^{N} \left[x_i' \right]^2} = \sqrt{\frac{1}{N} \sum_{i=1}^{N} \left[x_i - \overline{X} \right]^2} \quad , \qquad [B\text{-}5]$$

S_x Skewness;

$$\frac{\frac{1}{N} \sum_{i=1}^{N} \left[x_i' \right]^3}{\sigma_x^3} \quad , \qquad [B\text{-}6]$$

K_x Kurtosis;

$$\frac{\frac{1}{N} \sum_{i=1}^{N} \left[x_i' \right]^4}{\sigma_x^4} - 3 \quad , \qquad [B\text{-}7]$$